Evolution of the $j-1$ anomalous states of the j^{-3} multiplets

S. Lalkovski [1,*] and S. Kisyov [2]

[1]*Faculty of Physics, Sofia University "St. Kliment Ohridski," Sofia 1164, Bulgaria*
[2]*Lawrence Livermore National Laboratory, Livermore, California 94550, USA*

In the nuclear shell model the $j-1$ anomaly is associated with unusual ordering of the j and $j-1$ states of a j^{-3} split multiplet. In the mass regions placed away from the doubly magic nuclei, the $j-1$ levels are found to be below the respective j states. The anomalous ordering of the levels is most prominent in the silver isotopic chain, but a similar effect is observed also in other systems with pure three-hole configurations. The correlation between the $\Delta E = E_{j-1} - E_j$ energy splitting, observed in some odd-mass nuclei, and the even-even core's 2^+ level energy is well pronounced in the (28,50) neutron and proton shells and to a lesser extent in the lower and higher (20,28) and (50, 82) shells.

I. INTRODUCTION

The nuclear shell model [1] was introduced in the mid-twentieth century and quickly became one of the cornerstones of the contemporary nuclear physics owing its success, among others, to the description of the nuclear "magic" numbers. It is now well established that these magic numbers emerge due to the spin-orbit force [2,3], which at the medium-mass and heavy nuclei, decouples single-particle orbits from the upper shells and pushes them down in energy towards the shells where the majority of the single-particle states have opposite parities. This phenomenon is responsible for the magic gaps formation at occupation numbers 28, 50, 82, and 126, but also for the emergence of some subshell gaps, at $Z = 40$, for example, where extra stability towards nuclear excitation is observed. The single-particle orbits, responsible for the rearrangement of the shells and $\pi = (-1)^l$-parity intruder states appearance, are $l_j = f_{7/2}$, $g_{9/2}$, $h_{11/2}$, and $i_{13/2}$.

Historically, the nuclear shell model was developed to explain the structure of the nuclei placed on, or close, to the line of β stability and was parametrized with respect to these nuclei. However, some recent experiments suggest that the spin-orbit interaction might weaken and even vanish in the exotic neutron-rich regions, but variations of the spin-orbit strength is not a unique feature of the exotic nuclear regions. Already at the β-stability line, the spin-orbit interaction strength varies from shell to shell [4] and differs for proton and neutron nuclear components [4]. The net result is that the single-particle orbits ordering depends on the mass region and the type of nucleons considered.

The main focus of the present article is the silver nuclei. They are three proton holes away from the $Z = 50$ magic number where the intruder orbit is $\pi g_{9/2}$. This orbit is responsible for the subshell closure at $Z = 40$ and the appearance

of positive-parity states in the odd-Z nuclei there. Hence, it is natural to expect that this particular orbit plays a major role in the structure of the positive-parity low-lying states of Ag nuclei. Indeed, as shown in Fig. 1, the lowest-lying positive-parity state observed in $^{97}_{47}\text{Ag}_{50}$ [5–7] is $9/2^+$, which can be associated with $\pi g_{9/2}$ occupation. The next excited positive-parity state is $7/2^+$. Excitation across the shell gap could explain the state, but the $Z = 50$ shell gap width is approximately 4-MeV wide. Hence, occupation of the $\pi g_{7/2}$ orbit can not explain the appearance of this state at low energies. In the medium-mass silver nuclei the behavior of the $7/2^+$ is even more tantalizing [8,9] since it becomes the lowest-energy positive parity state as shown in Fig. 2. The reordering of the j and $j-1$ states is known as the $j-1$ anomaly.

II. j^{-3} COUPLING SCHEME

The idea of $7/2^+$ being a single-particle excitation was refuted as early as in the 1960s. At that time the experimental level energies of the most exotic neutron-deficient silver nucleus ^{97}Ag were unknown. This nucleus was not discovered until the late 1970s [16], but the $(7/2^+, 9/2^+)$ doublet reordering was already observed in the neutron midshell silver isotopes rising questions about the nature of the anomaly. In the 1960s, Kisslinger pointed out [17] that in such nuclei the anomalous ordering of j and $j-1$ levels can be generated by three-particles (or holes) single-j clusters.

The j^{-3} scheme is a direct derivative from the nuclear shell model [18]. The split seniority scheme arises from the residual interaction between the valence particles. The maximum spin of the multiplet depends on the single-particle orbit on which the three particle/holes are. In the case of the $g_{9/2}^{-3}$ configuration, the spectrum consists of states with angular momenta from $J^\pi = 3/2^+$ to $21/2^+$ except for the $19/2^+$ which is not part of the multiplet. All states, except for $9/2_1^+$ state which is the seniority $v = 1$ state, are $v = 3$ states [19]. The j^{-3}
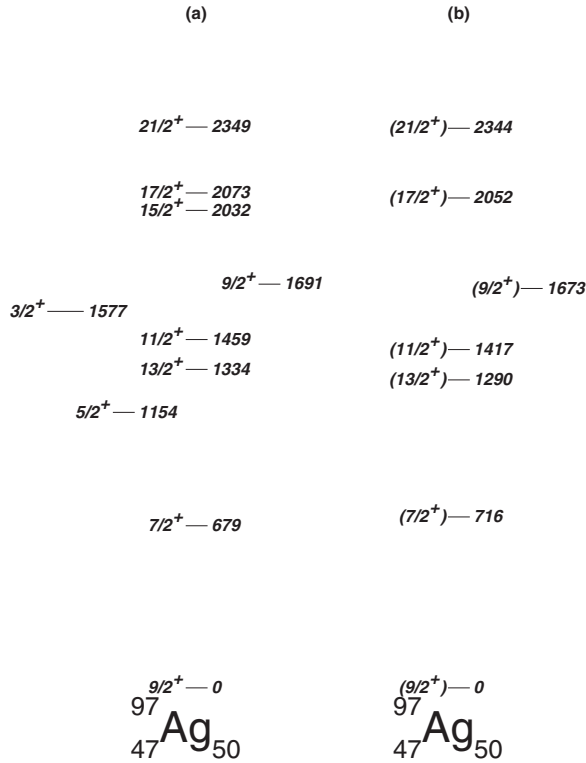
---
*s.lalkovski@phys.uni-sofia.bg

FIG. 1. (a) Theoretical $\pi g_{9/2}^{-3}$ and (b) experimental [5–7] $^{97}_{47}\text{Ag}_{50}$ level schemes.

spectrum [4] can be calculated from the two-body matrix elements $A_{J'}$ as

$$\langle j^3\alpha; JM|H|j^3\alpha; JM\rangle = 3\sum_{J'}[j^2(J')jJ|\}j^3J]^2 A_{J'}, \quad (1)$$
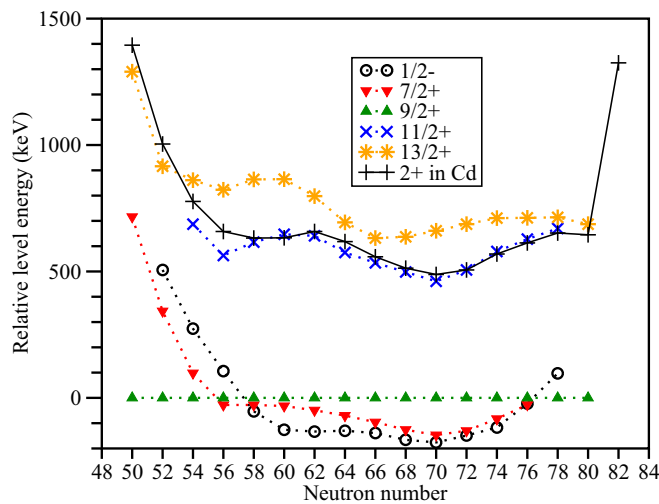

FIG. 2. Yrast states in Ag nuclei as a function of the neutron number. All level energies are relative to the $9/2^+$ level. Modified from Ref. [10], the figure accounts for the new data [11–15]. The 2^+ core energies are in absolute units, i.e., relative to the cadmium ground states.

TABLE I. Coefficients of fractional parentage for $j = 9/2$ [19,20].

J	v	$J' = 0$	$J' = 2$	$J' = 4$	$J' = 6$	$J' = 8$
3/2	3			2.18182	0.81818	
5/2	3		0.83333	0.59091	1.57576	
7/2	3		1.57576	0.41958	0.00606	0.99860
9/2	1	0.8	0.25	0.45	0.65	0.85
9/2	3		0.09848	1.28497	1.45606	0.16049
11/2	3		0.51515	1.18881	0.33939	0.95664
13/2	3		0.90909	0.18881	0.77273	1.12937
15/2	3			0.3986	1.90909	0.69231
17/2	3			0.87413	0.51818	1.60769
21/2	3				0.7	2.3

where $[j^2(J')jJ|\}j^3J]$ are the coefficients of fractional parentage (cfp). Here j denotes the single-particle total angular momentum; J' is the spin to which two of the particles couple; and J is the total three-particle angular momentum. Table I shows the cfps for three particles on $j = 9/2$ [19,20].

The two-body matrix elements $A_{J'}$ can be obtained from the neighboring even-even semi-magic nuclei with two valence particles or holes by using the Talmi procedure [4,18]. The recipe was followed in the ^{97}Ag level energies calculations where the two-body matrix elements $A_{J'} = \{0, 1395, 2082, 2280, 2428\}$ keV, were deduced from the $^{98}_{48}\text{Cd}_{50}$ [21] spectrum, assuming that the yrast states are of the pure $\pi g_{9/2}^{-2}$ nature. The calculated spectrum is shown in Fig. 1(a) and compared to experimental data in Fig. 1(b). The ordering of $9/2^+$ and $7/2^+$ levels as well as the energy gap are correctly reproduced. The higher-lying $13/2^+$, $17/2^+$, and $21/2^+$ yrast states appear also as they were experimentally observed in Ref. [22]. The $9/2_2^+$ and $11/2^+$ $v = 3$ states were also observed recently [7]. The remaining members of the j^{-3} multiplet are yet to be discovered, but the available experimental data on ^{97}Ag are consistent with the j^{-3} coupling scheme.

Alternatively, the two-body matrix elements $A_{J'}$ can be calculated by using effective quadrupole-quadrupole QQ or surface δ interactions (SDIs) [23]. These two interactions lead to two distinctive excitation patterns. The SDI interaction, which preserves [24] the seniority quantum number v, generates a $9/2^+$ ground state. Contrary to it, the QQ interaction does not preserve seniority and gives rise to the $7/2^+$ ground state. The experimental data, shown in Fig. 2, seem to indicate a transition between the two regimes. In ^{97}Ag, and the neighboring two isotopes, the $9/2^+$ state is the lowest-lying positive-parity state. For ^{103}Ag and heavier nuclei, the $9/2^+$ and $7/2^+$ states swap their places in accordance with the QQ interaction pattern. For those silver nuclei, up to ^{123}Ag, $7/2^+$ is the lowest in the energy positive-parity state. In ^{125}Ag, the two states are expected to swap once again places in accordance with the SDI pattern. However, the $7/2^+$ multiplet member is not discovered yet. If such scenario turns out to be valid, $^{129}_{47}\text{Ag}_{82}$ will have the typical seniority level scheme as shown in Fig. 3, which can be expected at the $N = 82$ shell closure by analogy with ^{97}Ag. The ^{129}Ag excited levels are not observed yet, but any deviation of the experimental data from
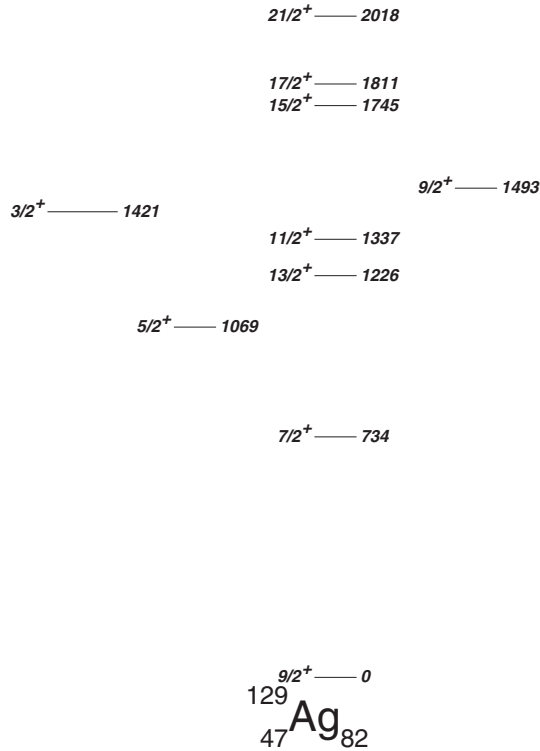
FIG. 3. $\pi g_{9/2}^{-3}$ calculations for $^{129}_{47}\text{Ag}_{66}$. The two-body $A_{J'} = \{0, 1325, 1864, 1992, 2130\}$-keV matrix elements are estimated from $^{130}_{48}\text{Cd}_{82}$ [25].
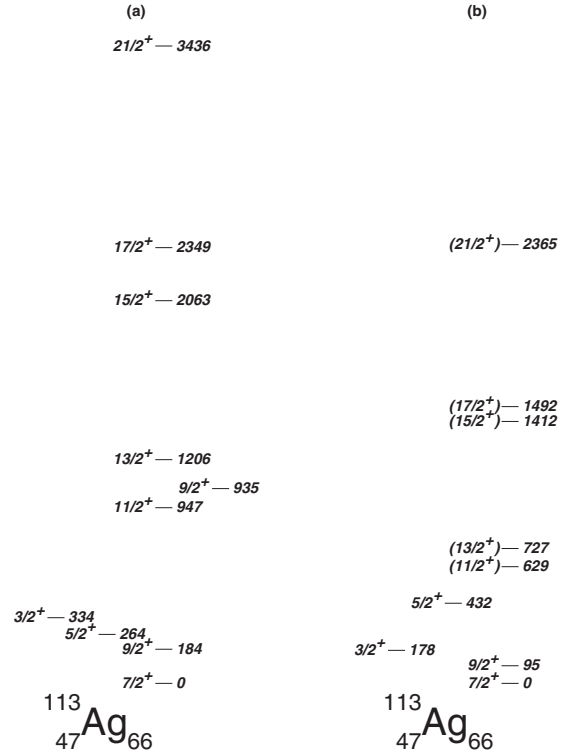

FIG. 4. (a) Theoretical $\pi g_{9/2}^{-3}$ and (b) experimental [12,28] $^{113}_{47}\text{Ag}_{66}$ level schemes. All level energies are relative to $E_{7/2^+}$.

the $\pi g_{9/2}^{-3}$ pattern would indicate departure from the classical shell structure in this neutron-rich mass region.

The smooth transition from SDI- to QQ-like regimes, observed in the experimental level energies of odd-mass silver nuclei, has been well reproduced by j^{-3} calculations. Figure 4 presents single-shell calculations for the neutron midshell $^{113}_{47}\text{Ag}_{66}$ nucleus parametrized with respect to the neighboring cadmium nuclei. Indeed, the calculations reasonably reproduce the low-energy spectrum of the nucleus having a typical seniority broken QQ-like level structure. Even though, the experimental spectrum resembles the decoupled rotational bands [26], the states emerging from the j^{-3} schemes are present, and the yrast states appear in the right order. A better description could be obtained by enlarging the model space by inclusion of the $\pi 2d_{5/2}$ orbit, which was found to have an effect on the $11/2^+$ and $13/2^+$ states [27]. Such an enlarged model space would also affect the low-spin $3/2^+$ and $5/2^+$ states which are more sensitive to the size of the model space and, hence, not properly described by the pure $\pi 1g_{9/2}^{-3}$ calculations, in the case of the neutron midshell ^{113}Ag.

It should be noted, however, that these calculations smear the effect of the neutron component on the residual interaction through the two-body terms calculated from the neighboring cadmium nuclei. Another downside of this approach is its incapability to explain the $M1$ transitions observed between the $j - 1$ and the j members of the j^{-3} multiplet [19]. As a consequence, large-space shell-model calculations were carried out for $^{123-129}\text{Ag}$ [10]. They were performed by taking

into account both the proton $\pi 1f_{5/2}$, $\pi 2p_{3/2}$, $\pi 2p_{1/2}$, and $\pi 1g_{9/2}$ and the neutron $\nu 1g_{7/2}$, $\nu 2d_{5/2}$, $\nu 2d_{3/2}$, $\nu 3s_{1/2}$, and $\nu 1h_{11/2}$ single-particle orbits. The modern jj45pna effective interaction, parametrized with respect to the $A = 132$ nuclei, was used. As a result, more complex wave functions were obtained, but the overall result was worse than that obtained from the three-single-j particle calculations. Nevertheless, these calculations had also shown that the $\pi g_{9/2}^{-3}$ configuration plays an important role in the formation of the positive-parity states in the silver nuclei placed away from the magic numbers.

Recently, truncated large-scale shell-model calculations were performed and compared to two-orbit shell-model calculations where only $\pi g_{9/2}^{-3} \otimes \nu h_{11/2}^m$ configurations were taken into account [11]. They show a better description of the positive-parity yrast states in $^{113,119,121}\text{Ag}$ isotopes, emphasizing the role of the $\nu h_{11/2}$ intruder orbit in the nature of the positive-parity yrast states in Ag isotopes.

III. PARTICLE(S)-CORE MODELS

A different approach has been exploited in the 1970s within a model based on vibrational field interacting with a cluster of three valence particles or holes [29]. The model succeeds in describing large set of states. The magnitude of the $(j, j - 1)$ splitting is strongly dependent on the cluster-core interaction strength, and the $j - 1$ anomaly has been found to emerge at large values of the interaction parameter.

Furthermore, in the 1970s, the axially symmetric-rotor-plus-particle model and the traixial-rotor-plus-particle model
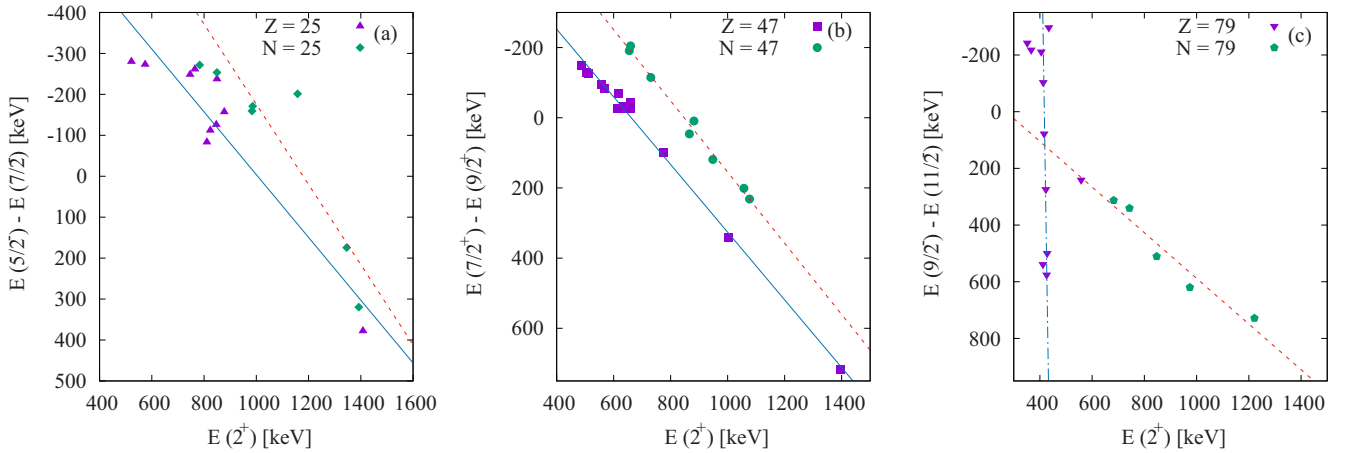
FIG. 5. Systematic of (a) $Z = 25$ and $N = 25$; (b) $Z = 47$ and $N = 47$; and (c) and $Z = 79$ and $N = 79$ data.

calculations were performed. Examples are presented in Refs. [30,31]. Within those models, the $j - 1$ anomaly is explained via a deformed core-particle interaction and triaxiallity. More recently, the structure of the midshell nuclei ^{111,113}Ag was studied within the interacting Boson-fermion model [12]. None of these approaches, however, can satisfactorily describe the structure of the low-lying states of the silver nuclei unless three hole clusters are taken into account.

IV. EXPERIMENTAL DATA

The systematic of the low-lying positive-parity states in the Ag isotopic chain, presented in Fig. 2, shows two overall distinctive regimes. In the light nuclei, placed close to the $N = 50$ magic number, $7/2^+$ appears above the $9/2^+$ state. There, the respective core energy is ≈ 1000 keV. When approaching the neutron midshell the core 2^+ level energy decreases from 600 to 300 keV. As a result, the $9/2^+$ and $7/2^+$ states swap their places, and $7/2^+$ becomes the lowest-lying positive parity state in the silver odd-mass nuclei. Thus, the position and

TABLE II. Experimental data for three-hole unique parity configurations to 28, 50, and 82 neutron and proton magic numbers. $E_{2_1^+}$ in keV is the level energy of the first excited state of the respective two-hole neighbor. $\Delta = E_{j-1} - E_j$ in keV is calculated from the $j - 1$ and j level energy differences. All energies are given in keV. The data are retrieved from Ref. [32] as of 30.09.2022.

$Z = 26$	^{50}Fe	^{52}Fe	^{54}Fe	^{56}Fe	^{58}Fe	^{60}Fe	^{62}Fe	^{64}Fe	^{66}Fe	^{68}Fe			
E_{2^+} (keV)	765	849	1408	847	811	824	877	746	574	522			
$Z = 25$	^{49}Mn	^{51}Mn	^{53}Mn	^{55}Mn	^{57}Mn	^{59}Mn	^{61}Mn	^{63}Mn	^{65}Mn	^{67}Mn			
Δ (keV)	-261	-237	378	-126	-83	-112	-157	-248	-273	-280			
$N = 26$	^{40}Si	^{42}S	^{44}Ar	^{46}Ca	^{48}Ti	^{50}Cr	^{52}Fe	^{54}Ni					
E_{2^+} (keV)	986	903	1158	1346	984	783	849	1392					
$N = 25$	^{39}Si	^{41}S	^{43}Ar	^{45}Ca	^{47}Ti	^{49}Cr	^{51}Fe	^{53}Ni					
Δ (keV)	-171	-449	-201	174	-159	-272	-254	320					
$Z = 48$	^{98}Cd	^{100}Cd	^{102}Cd	^{104}Cd	^{106}Cd	^{108}Cd	^{110}Cd	^{112}Cd	^{114}Cd	^{116}Cd	^{118}Cd	^{120}Cd	^{122}Cd	^{124}Cd
E_{2^+} (keV)	1395	1004	777	658	633	633	658	618	558	513	488	506	569	613
$Z = 47$	^{97}Ag	^{99}Ag	^{101}Ag	^{103}Ag	^{105}Ag	^{107}Ag	^{109}Ag	^{111}Ag	^{113}Ag	^{115}Ag	^{117}Ag	^{119}Ag	^{121}Ag	^{123}Ag
Δ (keV)	716	343	98	-28	-28	-32	-45	-70	-96	-126	-148	-130	-83	-27
$N = 48$	^{78}Zn	^{80}Ge	^{82}Se	^{84}Kr	^{86}Sr	^{88}Zr	^{90}Mo	^{92}Ru						
E_{2^+} (keV)	730	659	655	882	1077	1057	948	866						
$N = 47$	^{77}Zn	^{79}Ge	^{81}Se	^{83}Kr	^{85}Sr	^{87}Zr	^{89}Mo	^{91}Ru						
Δ (keV)	-115	-205	-191	9	232	201	119	46						
$Z = 80$	^{178}Hg	^{180}Hg	^{182}Hg	^{184}Hg	^{186}Hg	^{188}Hg	^{190}Hg	^{192}Hg	^{194}Hg	^{196}Hg	^{198}Hg			
E_{2^+} (keV)	558	434	352	367	405	413	416	423	428	426	412			
$Z = 79$	^{177}Au	^{179}Au	^{181}Au	^{183}Au	^{185}Au	^{187}Au	^{189}Au	^{191}Au	^{193}Au	^{195}Au	^{197}Au			
Δ (keV)	241	-297	-243	-218	-211	-103	78	274	500	576	539			
$N = 80$	^{130}Sn	^{132}Te	^{134}Xe	^{144}Gd	^{146}Dy									
E_{2^+} (keV)	1221	974	847	743	683									
$N = 79$	^{129}Sn	^{131}Te	^{133}Xe	^{143}Gd	^{145}Dy									
Δ (keV)	729	620	511	341	313									

the ordering of the $7/2^+$ and $9/2^+$ states are strongly correlated with the 2^+ level energy of the core. This effect is even more prominent in Fig. 5(b) where the $\Delta E = E_{7/2^+} - E_{9/2^+}$ level energy difference is plotted as a function of the core's E_{2^+}. As shown in Fig. 5(b), the $N = 47$ isotones follow a similar trend. In the $N = 47$ isotonic chain at low energies, the level schemes are also dominated by positive-parity states arising from $\nu g_{9/2}$ intruder orbit. Again, when the proton number is close to $Z = 50$, the $9/2^+$ level is the lowest-lying positive-parity state. In those nuclei the $7/2^+$ state is lying at higher energies. The experimental $\Delta E = E_{7/2^+} - E_{9/2^+}$ level energy splitting is given also in Table II as a function of the core's 2^+ level energy. Deeper in the proton shell where the deformation start to emerge, the two levels swap their places as is in the $Z = 47$ case.

Thus, at first glance, depending on the relative position with respect to the shell gaps, two excitation patterns can be distinguished. A j^{-3}-seniority scheme that can explain the behavior of the nuclei placed close to the shell edges, and a seniority-broken regime represented by a different level ordering. Thus, in the nuclei for which one of the two components (protons or neutrons) is close to the magic number, and the other is far away from the nearest shell gap, represent excitation features close to the j^{-3} configuration with phenomenological QQ interaction, and/or collective-particle(s) model description. The experimental data shown in Fig. 2, however, suggest a more gradual change between these two distinctive regimes.

Nevertheless, what emerges from the systematic in the present paper is that the $(9/2^+, 7/2^+)$ levels splitting of the $g_{9/2}^{-3}$ multiplet strongly depend on the core's 2^+ level energy, suggesting that the core excitation plays an important role already at low excitation energies throughout the entire silver isotopic chain.

The $(j, j-1)$ energy splitting as a function of the 2^+ core energy is plotted in Fig. 5(a) for a number of $N, Z = 25$ nuclei where the intruder orbit is $f_{7/2}$. The trend is similar to that of the silver isotopic chain, even though the correlation is weaker. Nuclear level energies of $Z, N = 26$ nuclei and $\Delta E = E_{j-1} - E_j$ for the odd-mass $Z, N = 25$ systems are also given in Table II.

In the upper $Z, N = 50$–82 shells, relatively pure j^{-3} three-particle systems can arise from $h_{11/2}$ single-particle orbit. These can be expected to occur in the $Z, N = 79$ nuclei. Level energy differences have been obtained from the first excited $11/2^-$ and $9/2^-$ states and plotted in Fig. 5(c) versus 2^+ level energies of the core mercury nuclei. The systematics

suggests that in the case of $Z = 79$ Au isotopes the correlation is broken which is probably due to the larger valence space and more complex wave functions.

It is interesting to note that whatever the mechanism is that generates the silver positive-parity yrast states, it is exhausted at $21/2^+$ in line with the $\pi g_{9/2}^{-3}$ scheme. Above this level, magnetic rotational bands are observed in several neutron midshell silver nuclei [33]—another effect also associated with spherical shapes. These spectroscopic findings are somewhat contradictory to the experimental quadrupole moments [34] of the $7/2^+$ states suggesting they are collective, hence, the bands on top of these states are also collective. In order to resolve the enigma, further data including nuclear lifetimes and precise mixing ratios of the electromagnetic transitions are needed.

V. CONCLUSION

The nuclear shell model and the particle-core models are two of the cornerstones in modern nuclear physics. Their success is based on the applicability of the adiabatic principle which allows to disentangle single-particle from collective modes. Thus, nuclei of well-pronounced shell-model behavior are located near the magic numbers, whereas nuclei with a large number of valence particles form the regions of collectivity on the nuclear landscape. Each of these regimes is characterized by few distinctive features. Such a feature is the seniority concept, which is well understood within the spherical shell-model space, but not when deformation is present. Yet, the data on the light and medium-mass systems seem to support a gradual evolution between the two regimes. Furthermore, the medium-mass silver isotopes seems to exhibit features that are more consistent with the spherical nuclei, even though quadrupole deformation start to develop in these nuclei. In the heavy-mass nuclei the correlation between the j and the $j-1$ components of the j^{-3} multiplet breaks, and the $(j, j-1)$ level energy splitting fails to strictly follow the core's 2^+ level energy. This is particularly valid for the $Z = 79$ Au isotopes.

[1] M. G. Mayer, Phys. Rev. **74**, 235 (1948).

[2] O. Haxel, J. H. D. Jensen, and H. E. Suess, Phys. Rev. **75**, 1766 (1949).

[3] M. G. Mayer, Phys. Rev. **78**, 16 (1950)

[4] K. L. G. Heyde, *The Nuclear Shell Model* (Springer-Verlag, Berlin, Heidelberg, GmbH, 1994).

[5] N. Nica, Nucl. Data Sheets **111**, 525 (2010), and references therein.

[6] G. Lorusso, A. Becerril, A. Amthor, T. Baumann, D. Bazin, J. S. Berryman *et al.*, Phys. Rev. C **86**, 014313 (2012).

[7] J. Park *et al.*, Phys. Rev. C **99**, 034313 (2019).

[8] K. Heyde and V. Paar, Phys. Lett. B **179**, 1 (1986).

[9] L. K. Peker, J. H. Hamilton, and P. G. Hansen, Phys. Lett. B **167**, 283 (1986).

[10] S. Lalkovski *et al.*, Phys. Rev. C **87**, 034308 (2013).

[11] Y. H. Kim *et al.*, Phys. Lett. B **772**, 403 (2017).

[12] S. Lalkovski, E. A. Stefanova, S. Kisyov, A. Korichi, D. Bazzacco, M. Bergstrom *et al.*, Phys. Rev. C **96**, 044328 (2017).

[13] H. Watanabe *et al.*, Phys. Lett. B **823**, 136766 (2021).

[14] J. Kurpeta, A. Abramuk, T. Rzaca-Urban, W. Urban, L. Canete, and T. Eronen *et al.*, Phys. Rev. C **105**, 034316 (2022).

[15] F. G. Kondev *et al.*, Chin. Phys. C **45**, 030001 (2021).

[16] T. Elmroth, E. Hagberg, P. G. Hansen, J. C. Hardy, B. Jonson, H. L. Ravn, and P. Tideman-Petersson, Nucl. Phys. A **304**, 493 (1978).

[17] L. S. Kisslinger, Nucl. Phys. **78**, 341 (1966).

[18] A. de-Shalit and I. Talmi, *Nuclear Shell Theory* (Academic Press, New York, London, 1963).

[19] P. Van Isacker (private communication) (2014).

[20] I. M. Band and Y. I. Kharitonov, At. Data Nucl. Data Tables **10**, 107 (1971).

[21] J. Chen and B. Singh, Nucl. Data Sheets **164**, 1 (2020).

[22] M. Lipoglavšek, M. Vencelj, C. Baktash, P. Fallon, P. A. Hausladen, A. Likar, and C. H. Yu, Phys. Rev. C **72**, 061304(R) (2005).

[23] A. Escuderos and L. Zamick, Phys. Rev. C **73**, 044302 (2006).

[24] P. Van Isacker and S. Heinze, Ann. Phys. **349**, 73 (2014).

[25] A. Jungclaus *et al.*, Phys. Rev. Lett. **99**, 132501 (2007).

[26] D. Bucurescu and N. V. Zamfir, Phys. Rev. C **95**, 014329 (2017).

[27] J. Jolie, P. Van Isacker, K. Heyde, J. Moreau, G. Van Landeghem, M. Waroquier, and O. Scholten, Nucl. Phys. A **438**, 15 (1985).

[28] J. Blachot, Nucl. Data Sheets **111**, 1471 (2010).

[29] V. Paar, Nucl. Phys. A **211**, 29 (1973).

[30] R. Popli, J. A. Grau, S. I. Popik, L. E. Samuelson, F. A. Rickey, P. C. Simms *et al.*, Phys. Rev. C **20**, 1350 (1979).

[31] A. W. B. Kolshoven *et al.*, Nucl. Phys. A **315**, 334 (1979).

[32] www.nndc.bnl.gov.

[33] S. H. Yao *et al.*, Phys. Rev. C **89**, 014327 (2014).

[34] N. Stone, Table of Nuclear Electric Quadrupole Moments, INDC(NDS)-0833 (IAEA, Vienna, 2021), https://www-nds.iaea.org/publications/indc/indc-nds-0833.pdf.